Available online at www.sciencedirect.com
ScienceDirect
Ocean Modelling 15 (2006) 177–199
Ocean Modelling
www.elsevier.com/locate/ocemod

Geographic distribution of the diapycnal component of thermohaline circulations in coupled climate models

Shan Sun [a,*], Rainer Bleck [b,1]

[a] NASA, Goddard Institute for Space Studies, 2880 Broadway, New York, NY 10025, United States
[b] Los Alamos National Laboratory, Los Alamos, NM 87545, United States

Received 23 May 2005; received in revised form 3 May 2006; accepted 4 May 2006
Available online 15 June 2006

Abstract

Data archives from four global coupled ocean–atmosphere models are used to construct maps of diapycnal mass flux through selected isopycnal surfaces in the model oceans. The maps illustrate location and strength of the up and downwelling limbs of thermohaline-forced overturning loops whose stability in the face of rising atmospheric carbon dioxide (CO_2) concentrations is of major concern in century-scale climate prediction. The up and downwelling limbs simulated by the four models for present-day greenhouse gas concentrations are compared with observational estimates. Predicted changes in the overturning brought about by gradually rising atmospheric CO_2 content are compared model-to-model. While all four models predict some decline in the rate of Atlantic overturning during CO_2-induced global warming, the geographic layout of the overturning circulations in each model is found to be insensitive to the changing climate.

1. Introduction

By accounting for more than one-third of the poleward heat transport on our planet, the oceanic thermohaline circulation (THC) plays an important role in regulating climate. Anticipated changes in THC strength are thus a key factor in predicting future climate conditions. Due to the present lack of direct observations of THC variability, coupled atmosphere–ocean general circulation models are one of the few tools available today for exploring feedback mechanisms between ocean and atmosphere which may be important contributors to both natural and externally forced climate variability.

Described as a "conveyor" by Broecker (1991), the THC is mainly buoyancy-driven even though, according to Bjerknes' circulation theorem, it requires some turbulent downward mixing of surface properties (i.e., warming of the *sub*surface ocean in the upward limb of the circulation) for its maintenance. In the interior ocean, away from surface buoyancy sources, water largely flows along potential density surfaces. Evaluating the modeled THC in a density framework therefore highlights the role of water mass conversion processes in maintaining

* Corresponding author. Tel.: +1 212 678 6031.
E-mail addresses: ssun@giss.nasa.gov (S. Sun), rbleck@giss.nasa.gov (R. Bleck).
[1] Present address: NASA, Goddard Institute for Space Studies, New York, NY, USA.

1463-5003/$ - see front matter © 2006 Elsevier Ltd. All rights reserved.
doi:10.1016/j.ocemod.2006.05.002

this circulation. The wide range of modeled responses of the Atlantic THC to gradual CO_2 doubling is troubling in this regard. In the third Intergovernmental Panel on Climate Change (IPCC) Assessment these responses ranged from zero change to a decline of 14 Sv, as illustrated in Fig. 9.21 of IPCC (Houghton et al., 2001).

Some studies suggest that the primary reason for the slowdown of the THC during global warming is the increased surface freshwater flux into the North Atlantic (Wiebe and Weaver, 1999; Dixon et al., 1999), while in other studies it is the surface warming trend that causes the THC to weaken (Mikolajewicz and Voss, 2000), or the combination of both factors (Thorpe et al., 2001). The fact that some models (Latif et al., 2000; Gent, 2001; Sun and Bleck, 2001a) do not show a slowdown of the Atlantic THC during gradual CO_2 doubling adds to the confusion.

Model intercomparison is an important tool for understanding climate variability, mainly because it provides at least a qualitative measure of uncertainty attributable to closure schemes for small-scale physical processes and numerical implementation details. The ongoing climate simulation experiments conducted for the IPCC fourth assessment provide an opportunity to analyze data from a variety of climate models with an eye on THC-related mechanisms in climate variability.

In this study, the three-dimensional THC in four US-based climate models is analyzed using tools originally developed for diagnosing circulations in isopycnic coordinate models. The discovery that these tools can be applied to z coordinate model output allows us to draw into this intercomparison results from a variety of "mainstream" climate models. At the time of this writing, we have analyzed results from four climate models, namely, those developed at the Geophysical Fluid Dynamics Laboratory (GFDL) and the National Center for Atmospheric Research (NCAR), as well as two models developed at the Goddard Institute for Space Studies (GISS). One of the latter two models uses a hybrid-coordinate, but primarily isopycnic, ocean model.

2. Method

Ocean modelers have traditionally relied on a single tool for displaying the strength of the meridional overturning circulation (MOC) in their models, namely, the overturning streamfunction for the zonally integrated flow in individual basins in latitude-depth space. In an effort to replicate results often seen in publications by observationalists and inverse modelers (Schmitz, 1995; Macdonald and Wunsch, 1996; Ganachaud and Wunsch, 2000), Sun and Bleck (2001b) and Bleck and Sun (2004) developed a method for extracting quantitative geographic details of the 3-D thermohaline circulation in potential density space from model output. (The quantitative "conveyor" schematic shown in Fig. 1 was produced with this method.) Their early work

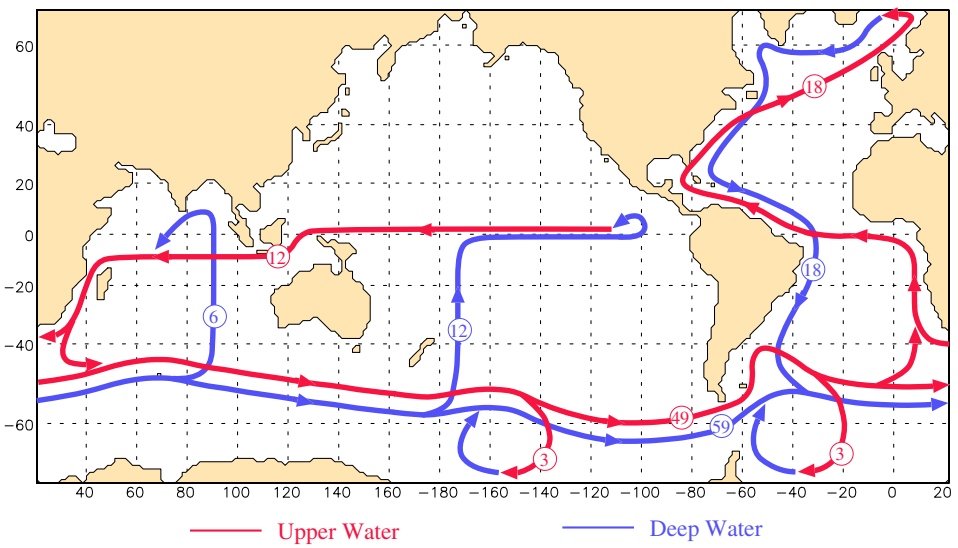

Fig. 1. Simplified schematic of the "deep" global thermohaline circulation in the isopycnal ocean model of Sun and Bleck (2001b), in a format inspired by Broecker (1991) and Schmitz (1995). Circled numbers represent transport in Sv ($1\ \text{Sv} = 10^6\ \text{m}^3\ \text{s}^{-1}$).

benefited from the predominantly isopycnic character of the ocean models used. The present study is the first in which geographic details of the THC are extracted from z coordinate model output. (Elements of this technique have previously been employed by Hu et al. (2004) in determining the iso/diapycnal mass fluxes passing through several prescribed control volumes in z coordinate model solutions.)

The idea underlying our method is to extract the diapycnal component of a model's 3-D mass flux field by vertically transforming time-averaged horizontal mass fluxes from each model's native vertical grid to isopycnic (potential density) coordinates. The missing diapycnal mass flux component is subsequently solved for as a residual from the time-averaged isopycnic-coordinate form of the continuity equation. Details of this procedure are as follows.

In generalized vertical coordinates (denoted here by the letter s), mass continuity in a hydrostatic fluid can be expressed as:

$$\frac{\partial}{\partial t}\left(\frac{\partial p}{\partial s}\right)+\nabla_s\cdot\left(\mathbf{v}\frac{\partial p}{\partial s}\right)+\frac{\partial}{\partial s}\left(\dot{s}\frac{\partial p}{\partial s}\right)=0, \tag{1}$$

where p is pressure, ∇_s is the two-dimensional gradient operator on an s surface, $\mathbf{v}$ is the horizontal velocity vector, and $\dot{s}\equiv \mathrm{d}s/\mathrm{d}t$ is the vertical velocity in s space. This equation states that the amount of mass ∂p enclosed between two s surfaces, spaced ∂s apart, changes with time due to the effect of horizontal (term 2) and vertical (term 3) mass flux divergences. Note that (1) is dimensionally consistent regardless of the definition of s, but since $\dot{s}$ does not necessarily have an easily understood physical meaning, it is customary to associate vertical motion with the product $\dot{s}\partial p/\partial s$.

Integration of (1) over the interval enclosed by two coordinate surfaces, say, $s=1$ and $s=2$, yields:

$$\frac{\partial}{\partial t}\Delta p+\nabla_s\cdot(\overline{\mathbf{v}}\Delta p)+\left(\dot{s}\frac{\partial p}{\partial s}\right)_2-\left(\dot{s}\frac{\partial p}{\partial s}\right)_1=0,$$

where the overbar denotes an average over $\Delta p=p_2-p_1$. (Complications arising from altering the order of differentiation, or from interchanging differentiation and integration, are avoided here by including both sea surface and ocean floor in the set of s coordinate surfaces.) Integrating the last equation over a finite time interval $\Delta t=t_{\mathrm{new}}-t_{\mathrm{old}}$ gives

$$(\Delta p)_{\mathrm{new}}-(\Delta p)_{\mathrm{old}}+\nabla_s\cdot\overline{(\overline{\mathbf{v}}\Delta p)}^{\Delta t}+\overline{\left(\dot{s}\frac{\partial p}{\partial s}\right)_2}^{\Delta t}-\overline{\left(\dot{s}\frac{\partial p}{\partial s}\right)_1}^{\Delta t}=0, \tag{2}$$

where time integrals are denoted by overbar-Δt.

If the change of layer thickness Δp with time and the time- and layer-integrated horizontal mass fluxes $\overline{(\overline{\mathbf{v}}\Delta p)}^{\Delta t}$ are known, the time-integrated vertical mass flux $\overline{(\dot{s}\partial p/\partial s)}^{\Delta t}$ across a given s surface can be determined by summing up (2) vertically, making use of the fact that $\dot{s}\partial p/\partial s=0$ at the top and bottom of the water column.

Sun and Bleck (2001b) designed an algorithm for integrating fields of diapycnal velocity, $\dot{\rho}\partial z/\partial\rho$, over regionally distinct "patches" of up or downwelling. This algorithm, which yields the total mass flux associated with each patch, vastly reduces the amount of data that need to be correlated with other elements of air–sea interaction. Use of this algorithm is an essential part of our work.

A side product of the coordinate transformation are the *horizontal* components of the 3-D mass flux vector in potential density space. These are often useful for providing a 3-D context for the diapycnal fluxes. By "bundling" horizontal mass fluxes, i.e., combining neighboring fluxes of equal sign into single strands, we have been able to construct schematics like the one shown in Fig. 1. See Bleck and Sun (2004) for further details.

The primary difficulty in processing results from multiple ocean models turned out to be the necessity to evaluate horizontal mass fluxes in exactly the form in which they are used to solve the continuity equation in the respective model. A precise knowledge of how the product of velocity components and horizontal map scale factors is formed on a staggered grid, for example, is essential. Complications arising from the use of partial bottom cells in z coordinate models, where applicable, must be fully taken into account. Given that layer models typically use flux limiters to assure positive-definiteness of layer thickness while solving the

continuity equation, the task of reconstructing lateral mass fluxes offline from given velocity and layer thickness fields is even harder in layer than in fixed-grid models. In HYCOM, one of the ocean models used in this study, mass fluxes are therefore part of the standard suite of output fields. Note that mass fluxes in HYCOM's isopycnic subdomain incorporate a bolus flux component induced by interface smoothing – the procedure underlying the GM (Gent and McWilliams, 1990) subgrid scale eddy mixing parameterization.

The need to (i) access "raw" output from models residing at multiple institutions and (ii) replicate each model's finite-difference expressions for solving the continuity equation is a definite impediment to the wide use of the analysis tool presented here. Nevertheless, we plan to extend this work to other models, including some at climate prediction centers outside the US.

3. Models

Data from four models are analyzed, see Table 1. Two models, GISS EH (GISS HYCOM, Sun and Bleck, 2006) and GISS ER (Russell et al., 2000) are from the Goddard Institute for Space Studies. They share the same AGCM (Schmidt et al., 2006) which has a horizontal resolution of $4^\circ \times 5^\circ$ and 20 vertical layers. The ocean model HYCOM (Bleck, 2002, 2006) uses a hybrid coordinate with isopycnal layers in the interior that transition to z layers near their outcrop location. This model was configured for the IPCC runs on a $2^\circ \times 2^\circ\cos(\textit{latitude})$ horizontal mesh and 16 vertical layers. Near the 60°N parallel, the Mercator projection gives way to a bipolar projection with poles placed in Canada and Siberia. The ocean component in GISS ER has the same horizontal resolution as the GISS AGCM and uses 13 vertical layers.

The GFDL model used here is version CM2.1 (Delworth et al., 2006; Gnanadesikan et al., 2006; Stouffer et al., 2006). The atmospheric model has a horizontal resolution of $2.5^\circ \times 2^\circ$ and 24 levels in the vertical. The ocean model resolution is 1° both in latitude and longitude, with meridional resolution gradually increasing to 1/3° equatorwards of ±30° latitude. Like in HYCOM, the grid degeneracy near the North Pole is avoided by transitioning to a bipolar projection.

The NCAR model used here is version CCSM3 (Bryan et al., 2006; Collins et al., 2006; Danabasoglu et al., 2006). The atmospheric horizontal resolution is T42 with an equivalent grid spacing of about 2.8° in latitude and longitude. There are 26 levels in the vertical. In the ocean model, the zonal resolution is 1.125°; the meridional resolution varies between 0.27° at the equator and 0.54° in the extratropics, and there are 40 levels in the vertical. Pole problems are avoided in this model by distorting the latitude–longitude grid in a way that moves the North Pole into the center of Greenland.

None of the four models analyzed here employ surface flux adjustments.

4. Results

The results presented below have been obtained by mapping horizontal mass fluxes in all four models from their original vertical coordinate onto the 16 potential density layers that serve as "target" densities in GISS EH. These values are listed in Table 2. The fact that over most of the ocean HYCOM's coordinate layers match the listed target densities and hence are not subject to vertical remapping could conceivably put HYCOM at an advantage as far as robustness of results is concerned. However, the fact that all four models show mutually consistent behavior leads us to believe that this potential advantage is inconsequential.

Table 1
General description of four models used in this study

Model	Znl × Merid. resolution	Points in lon/lat	Layers	Vert. coordinate	Sfc mix. lyr
GISS EH	$2^\circ \times 2^\circ\cos$ (lat)	180/181	16	Mainly isopycnal	KT
GISS ER	$5^\circ \times 4^\circ$	72/46	13	z-Level	KPP
GFDL CM2.1	$1^\circ \times (1/3^\circ$ to $1^\circ)$	360/200	50	z-Level	KPP
NCAR CCSM3	$1.125^\circ \times (0.27^\circ$ to $0.54^\circ)$	320/384	40	z-Level	KPP

KT stands for the Kraus–Turner slab surface mixed layer model (Kraus and Turner, 1967) and KPP the K profile parameterization (Large et al., 1994).

Table 2
The 16 σ_2 values in kg m^{-3} (potential density anomaly referenced to 2 km depth) used in the analysis

Layer	1	2	3	4	5	6	7	8
σ_2	30.90	31.87	32.75	33.54	34.24	34.85	35.37	35.80
Layer	9	10	11	12	13	14	15	16
σ_2	36.15	36.43	36.65	36.82	36.95	37.05	37.13	37.20

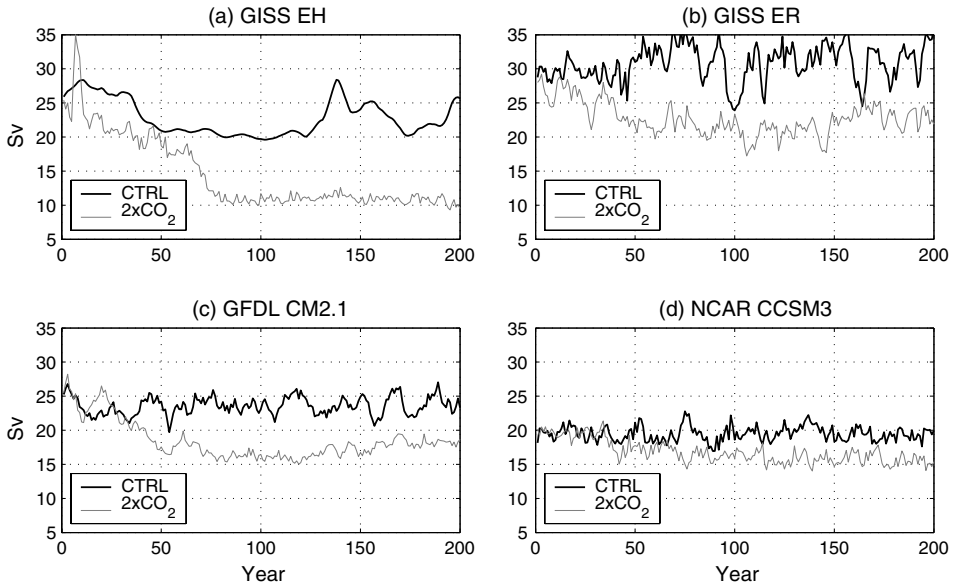

Fig. 2. Maximum overturning rate in the Atlantic over 200 years in the control and CO_2 doubling run in four models.

Fig. 2 shows the maximum overturning rate in the Atlantic over 200 years in the control and CO_2 doubling run for the four models. The maximum overturning strength is relatively stable in the CO_2 doubling run in all models, but there are different modes of decadal variability.

The IPCC protocol called for model predictions to be extended for 150 years past the doubling time of atmospheric CO_2, rising at a rate of 1% annually. In an effort to analyze flow fields representing the predicted $2 \times CO_2$ equilibrium climate, we selected data averaged over years 200–210, counting from the date at which CO_2 concentration begins to rise, and on the corresponding period from the control run. In the case of the GFDL model, where data from this period were unavailable to us, we use an average over years 190–200.

Note that all models except NCAR CCSM3 started from an initial CO_2 concentration representing pre-industrial conditions. The NCAR CCSM3 data available to us, on the other hand, were based on present-day CO_2 concentration as initial condition. In view of the work by Dixon and Lanzante (1999), who find that global warming and the strength of their modeled THC in the 21st century is insensitive to 1766, 1866 and 1916 choices for model initiation, we ignore the differences in the absolute CO_2 level in the four models in this study.

4.1. Mass field structure

To set the stage for the discussion of circulation-oriented diagnostics, let us take a brief look at how the mass field evolves in the four models over the course of 200 years. To this end, we show in Fig. 3 the zonally averaged depth of the 16 isopycnic layers listed in Table 2 at the completion of the 200-year control runs. The

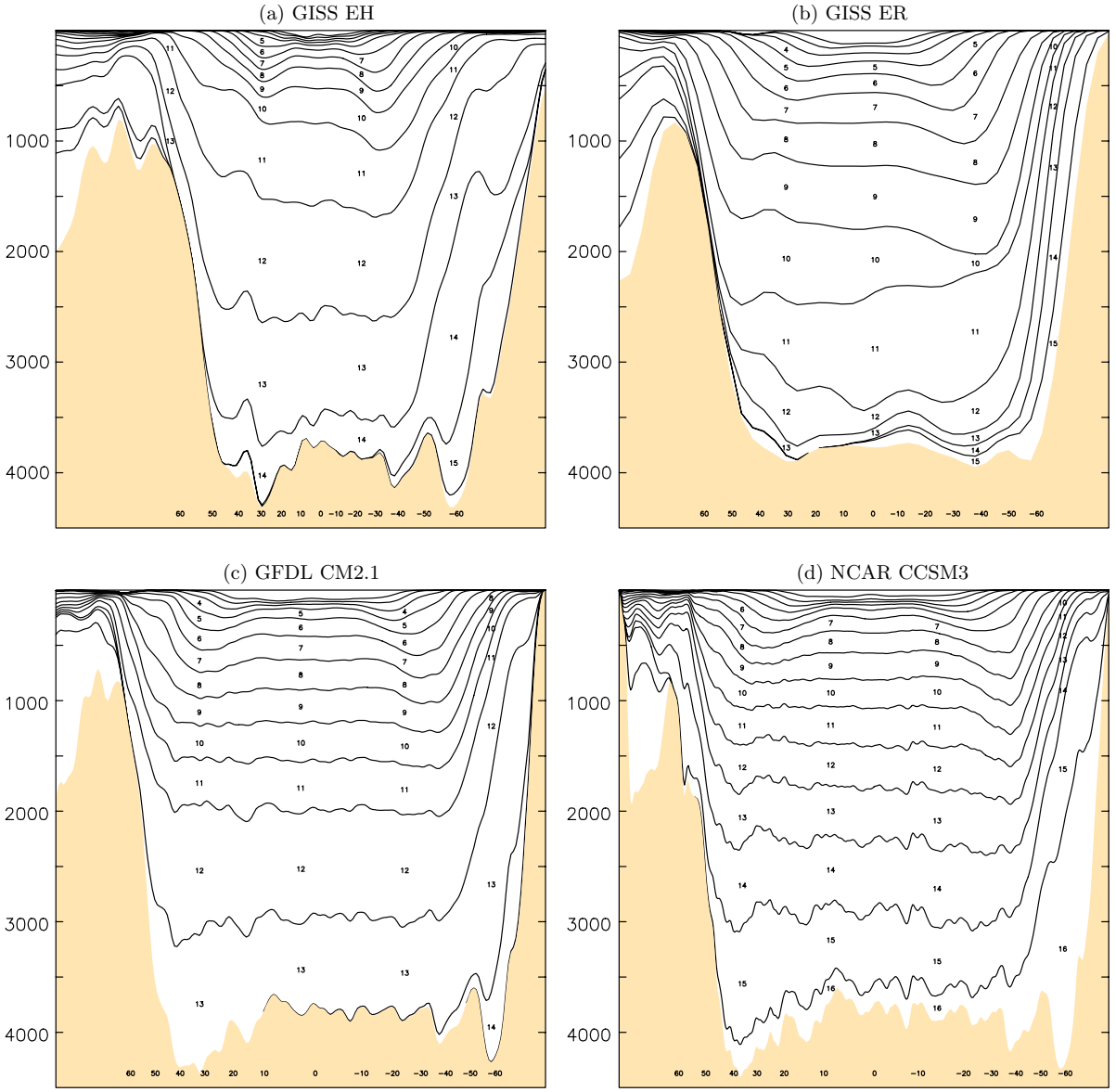

Fig. 3. Zonally averaged meridional cross sections through four model oceans at year 200 of the control run, showing depths of 16 isopycnal layers defined in Table 2. North is to the left. Note different abscissa scales.

corresponding layer depths extracted using observations PHC 3.0, which is an update of Steele et al. (2001), are shown in Fig. 4. These represent the initial conditions which the four models ideally should not deviate from.

Signs of model drift are hard to overlook. In the HYCOM ocean in GISS EH (Fig. 3a) isopycnals in the top 1000 m are seen to be displaced upward, resulting in a thermocline that is too shallow and too stratified compared to present-day observations. Note that upward/downward motion of isopycnals is equivalent to local density increase/decrease in z space. In the deeper ocean, layers have expanded downward, taking over the space originally held by layer 16 which no longer exists by year 200.

The density structure in GISS ER (Fig. 3b) reveals large downward movement of isopycnals at most depths and enhanced stratification just above the bottom. The frontal zone associated with the Antarctic circumpolar current (ACC) is displaced southward and spans the total basin depth, a feature not seen in Fig. 4.

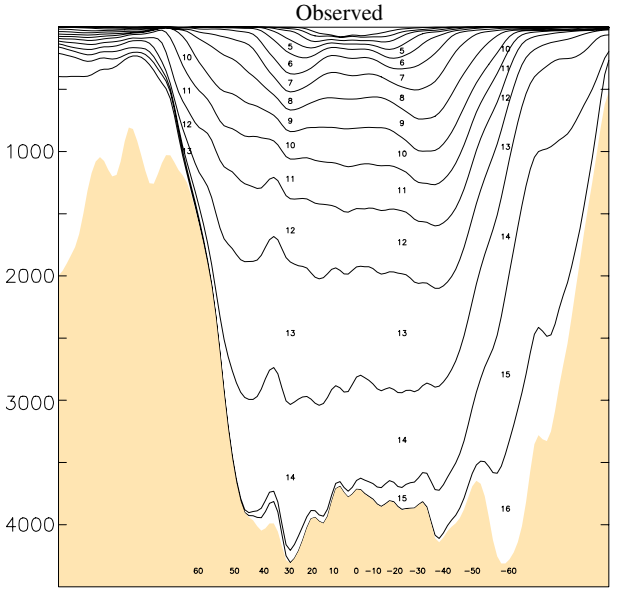

Fig. 4. Same as Fig. 3, but showing observations using PHC 3.0 (update of Steele et al., 2001).

The GFDL CM2.1 model solution (GFDL for short, Fig. 3c) is also characterized by downward migration of isopycnals at most depths. Stratification trends with depth match those seen in Fig. 4, but the density in the deep ocean is too low by at least one coordinate layer index. In fact, both layers 15 and 16 have vanished by year 200.

The NCAR CCSM3 model solution (NCAR for short, Fig. 3d) reveals little systematic vertical migration of isopycnals in the upper half of the ocean but a thinning of deeper layers to make room for a growing layer 16. (NCAR is the only model capable of replenishing layer 16.) The observed undulating interface pattern in the 500–2000 m depth range at low latitudes seen in Fig. 4, mainly created by equatorial upwelling in concert with subtropical downwelling, is slightly too weak in all z model runs.

4.2. Overturning stream functions

Figs. 5–8 show the overturning stream function in three basins and the global ocean, averaged over years 200–210 for GISS EH, GISS ER and NCAR CCSM3, and over years 190–200 for GFDL CM2.1. For easier reference to results presented later, we display the stream functions in latitude-σ_2 space rather than the more conventional latitude-z space. (Qualitative conversion to z space is possible by referring in Fig. 3.) Upper and lower panels in each figure show results from the control and CO_2 doubling experiment, respectively.

Three of the four models considered here use a computational mesh which at high northern latitudes deviates significantly from a spherical grid. Construction of truly meridional stream functions therefore would require converting mass fluxes from various native grids to latitude–longitude space. We decided against carrying out this conversion, because the associated interpolation errors would have interfered with attempts to (a) compare model behavior quantitatively and (b) cross-reference results obtained with different analysis tools. Hence, in three of the four models, the stream functions shown in Figs. 5–8 are not truly meridional at high northern latitudes. One particular process which they reveal limited or distorted information on is the overflow across the Greenland–Scotland ridge. We will make up for the lack of detail in the overflow region by switching to a different analysis tool, see Section 4.4.

The salient features seen in Figs. 5–8 are as follows:

1. In the control experiment, all four models show an Atlantic overturning rate, sampled at 50°N, of 17–24 Sv. These numbers are in good agreement with observational estimates (Schmitz, 1995; Macdonald and

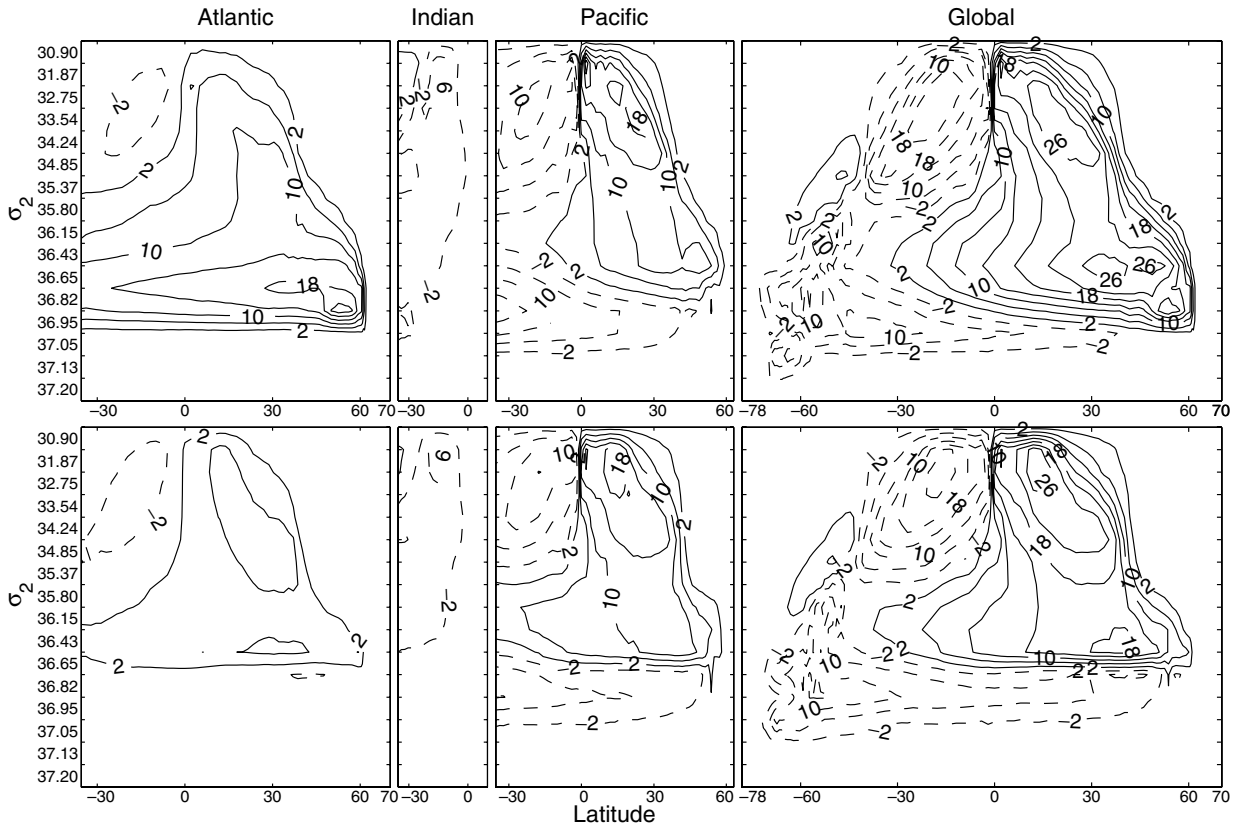

Fig. 5. Overturning stream function in three basins and global ocean in σ_2 coordinates (potential density referenced to 2 km) at year 200 for the control (upper) and CO_2 doubling experiment (lower) in GISS EH. Contour interval is 4 Sv, but contour lines are offset from zero by 2 Sv.

Wunsch, 1996; Ganachaud and Wunsch, 2000; Talley et al., 2003). The bulk of the deep southward flow takes place in layers $\sigma_2 = 36.82$ and 36.95, except in GISS ER where the flow is shifted up by one layer index to densities 36.65 and 36.82. In the NCAR model, some of the deep water formed in the North Atlantic is dense enough to return southward in the $\sigma_2 = 37.05$ layer. (As commented on in the previous section, the NCAR model seems most capable of creating very dense water.)

2. Inflow of Antarctic bottom water into the Atlantic varies from near-zero in GISS EH to 4 Sv in NCAR.
3. There is considerable variation in the amount of inflow of deep water from the Southern Ocean into the Pacific. The strongest inflow is seen in GISS EH with 15 Sv, followed by NCAR with 8 Sv. Inflow in the other two models does not exceed 3 Sv. The extreme GISS EH behavior is a well-understood consequence of lack of southern ice which spawns a strong thermally direct overturning cell in the southern hemisphere. Upgraded physics parameterizations have alleviated the ice loss in more recent runs that unfortunately did not meet the IPCC deadline.
4. The global stream function patterns from NCAR and GFDL show a distinct overturning cell between 40°S and Antarctica. Information in the IPCC data base provided by GFDL indicates that this cell can be reduced (though not eliminated) by taking into account bolus mass fluxes generated by the GM parameterization. Interface smoothing, the "natural" variant of the GM scheme suitable for isopycnic models, does not create overturning cells of the kind seen in Figs. 7 and 8, according to our experience. We will return to this issue at the end of the next section.
5. In the CO_2 doubling scenario (lower panels in Figs. 5–8), all models show some weakening of the Atlantic overturning. The decrease ranges from 4 Sv in GISS ER and NCAR to 12 Sv in GISS EH. The large decrease in GISS EH is somewhat disconcerting, given that earlier simulations (Sun and Bleck, 2001a)

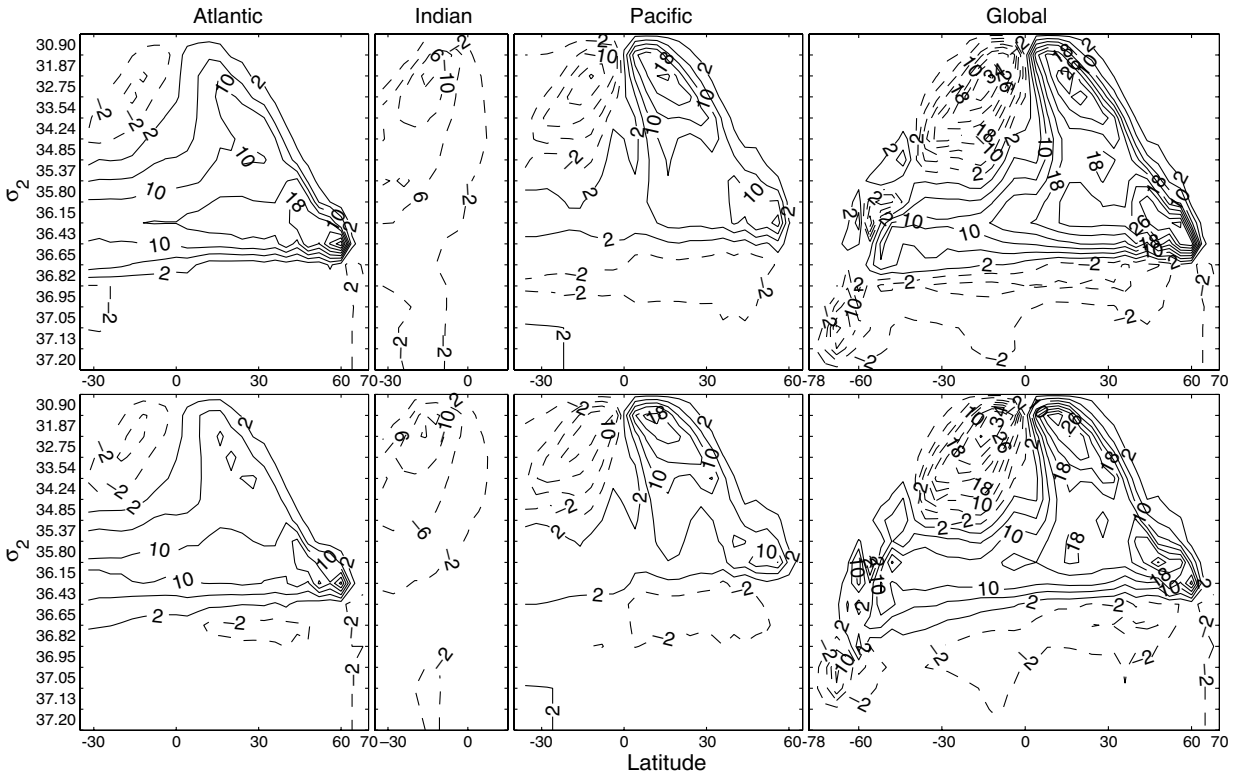

Fig. 6. As in Fig. 5, but for GISS ER model.

did not show a decline of the Atlantic MOC during CO_2 doubling at all. The discrepancy is largely due to recent numerous model changes, including the addition of a dynamic ice model. Similar evolutions have also been found in the NCAR model by Gent (2001) and Bryan et al. (2006). It is fair to say that we are still far from reliably predicting the fate of the THC during CO_2-induced global warming.

Readers trying to reconcile the above findings with stream function data submitted to the IPCC data base should be reminded that stream functions constructed in z space do not necessarily match the maxima and minima of those constructed in potential density space. While vertical remapping alone cannot create new flux maxima or minima in individual water columns, zonal summation of meridional fluxes can, because it draws on data from different depth levels. This can lead to an increase in the diagnosed overturning rate because thermally asymmetric (i.e., heat-transporting) horizontal circulation loops, which do not impact a stream function analyzed in z space, acquire a "vertical" component if analyzed in density space.

In order to calculate smoothly varying individual stream functions for the Pacific and Indian Ocean, the source/sink introduced by the Indonesian throughflow has been compensated in Figs. 5–8 by adding a clockwise circulation around Australia equal and opposite to the throughflow. The values of the Indonesian throughflow in each model are shown in Table 3 for the control and CO_2 doubling run.

Also shown in Table 3 is the strength of the ACC measured across the Drake Passage in each model. All models appear to overestimate this transport, except for GFDL which comes close to the observational estimate of 123 ± 11 Sv (Whitworth and Peterson, 1985), and 134 ± 11.2 Sv (Cunningham et al., 2003). In none of the models does the ACC transport change by more than $\pm 10\%$ in the CO_2 doubling case. The strength of the Drake Passage transport is set by a complex interplay of buoyancy forcing, wind forcing, and bottom drag (e.g., Olbers et al., 2004), and while the changes seen in Table 3 conceivably are linked to shifts in wind stress (see Fyfe and Saenko, 2005), we do not see a consistent response to global warming in the strength of the Drake Passage transport in the four models.

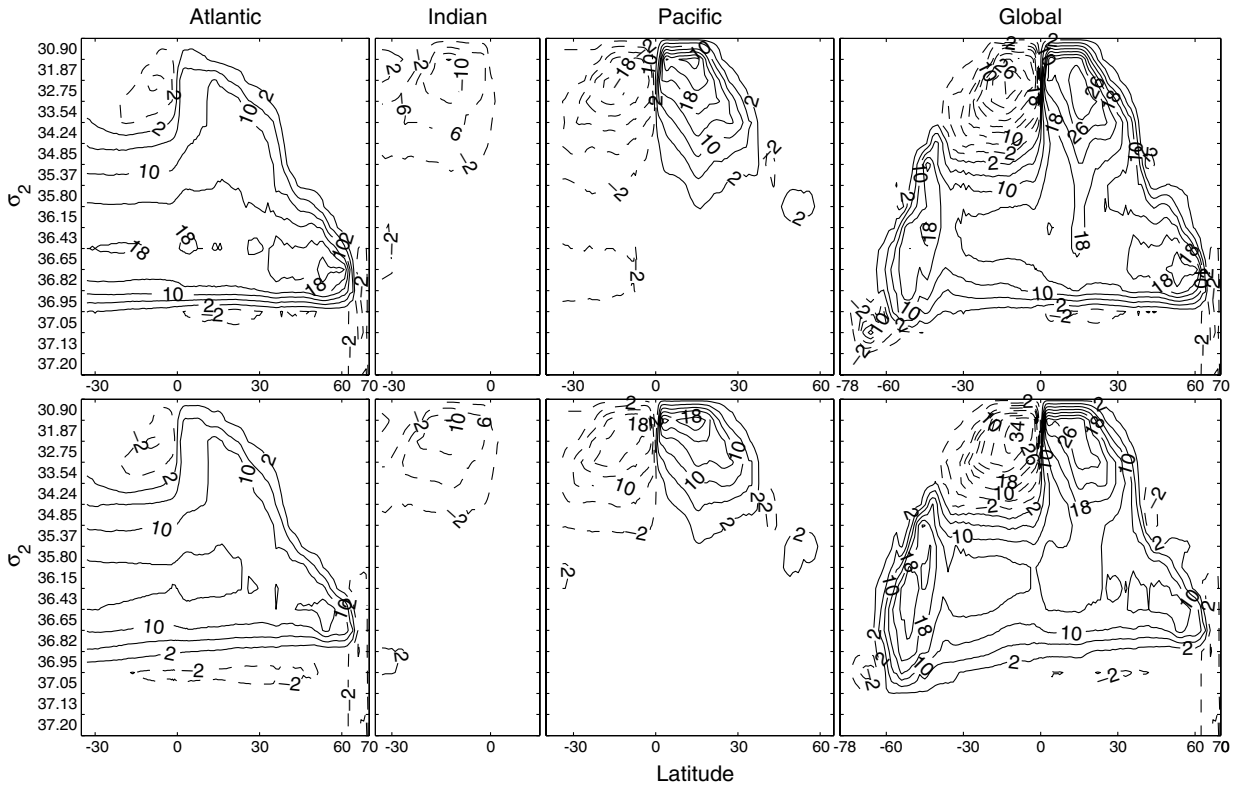

Fig. 7. As in Fig. 5, but for GFDL CM2.1 model.

4.3. Diapycnal fluxes

The centerpiece of our diagnostic effort are maps showing the geographic location and strength of the diapycnal limb of thermohaline-forced overturning circulations in the four models. These plots represent a step up, in terms of detail, from conventional basin-integrated stream function diagnostics. In order to preserve information about zonal/meridional grid resolution biases caused by map projections, we plot results in each model's actual grid point space.

Beginning with the control experiment in GISS EH, the upper panel in Fig. 9 shows the diapycnal fluxes across the interface between layers 11 and 12 ($\sigma_2 = 36.65$ and 36.82) in the control run, which according to Fig. 5 is the level coinciding with the stream function maximum in the North Atlantic. The figure shows that the diapycnal motion in the northern North Atlantic integrates to a total of 20 Sv (21 down, 1 up), broadly in agreement with Fig. 5. In the Southern Ocean beyond 45°S, the fluxes integrate to 20 Sv up and 28 Sv down, respectively. Within the error limits posed by the somewhat chaotic stream function plots, the net downward flux of 8 Sv matches the stream function value on the layer 11/12 interface at 45°S in the upper right panel in Fig. 5. Interestingly, the largest patch of diapycnal downwelling in the Southern Ocean is associated with an anticyclonic meander in the Antarctic circumpolar current (ACC) directing relatively warm water (i.e., water prone to heat loss) into the vicinity of the Ross Sea.

Other features in Fig. 9 (upper panel) worth noting are 6 Sv of net downwelling (12 down, 6 up) in the region surrounding the Kamchatka peninsula, and broadly distributed upwelling in the Pacific at a total rate of 23 Sv. Taking into account the 3 Sv downwelling off Taiwan, we arrive at a net upwelling rate for the Pacific of 14 Sv, in agreement with the value shown in the Pacific panel in Fig. 5.

In the CO_2 doubling run, the 6 Sv Atlantic overturning rate seen in the lower panel in Fig. 5 is composed, according to the lower panel in Fig. 9, of 10 Sv downwelling south of Iceland and off Norway on the one hand, and 4 Sv upwelling in the Labrador Sea and south of the Irminger Sea on the other hand.

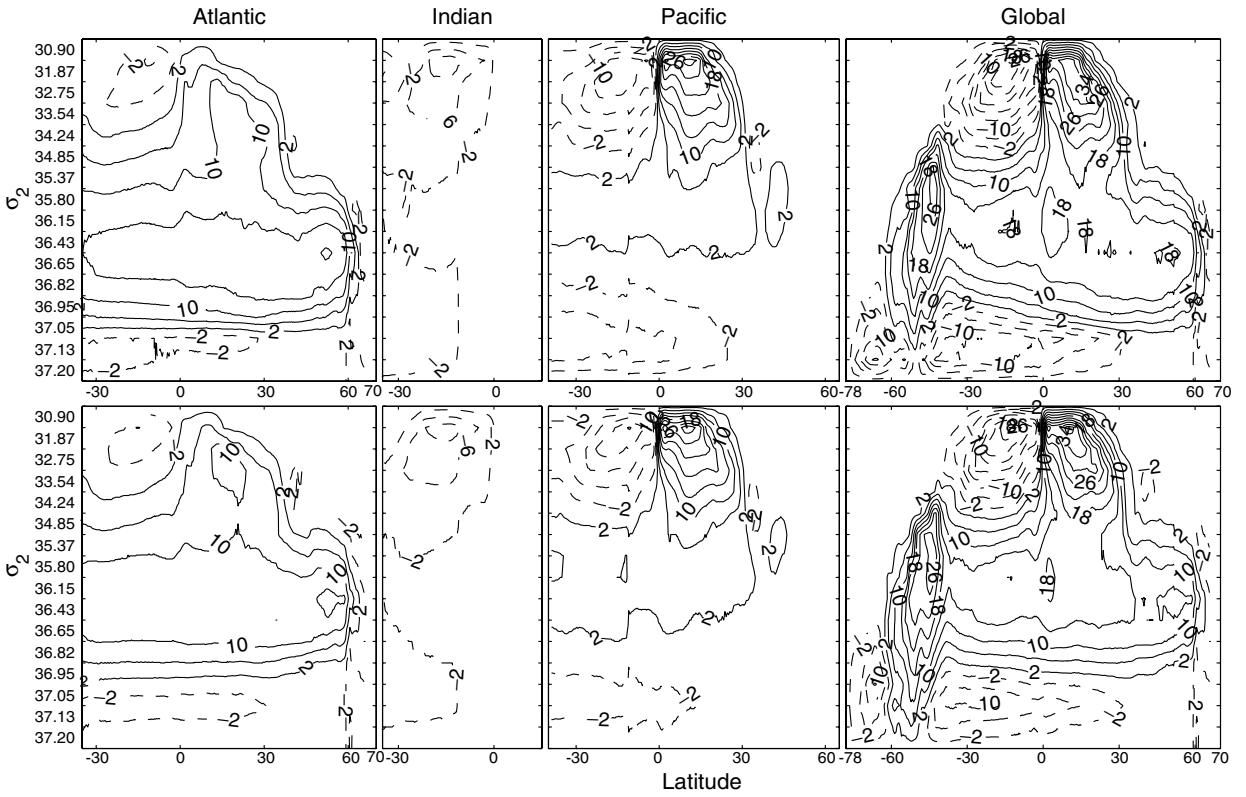

Fig. 8. As in Fig. 5, but for NCAR CCSM3 model.

Table 3
Indonesian throughflow and Drake Passage transport (Sv) in the control and 2 × CO_2 run in four models at year 200

	GISS EH		GISS ER		GFDL CM2.1		NCAR CCSM3	
	CTRL	2 × CO_2	CTRL	2 × CO_2	CTRL	2 × CO_2	CTRL	2 × CO_2
Indo. passage	12.3	7.0	7.1	6.4	13.5	10.0	14.2	11.0
Drake passage	161.9	170.9	223.4	236.2	131.4	127.8	177.7	165.8

The 18 Sv overturning rate at 50°N in the GISS ER control run (Fig. 6, upper panel) is shown in the upper panel in Fig. 10 to result from 28 Sv downwelling in and east of the Irminger Sea, and 11 Sv upwelling immediately to the south. A 5–6 Sv zonal overturning cell spans the Pacific with upwelling in the Gulf of Alaska. These diapycnal fluxes are weaker in the CO_2 doubling run, but the locations remain the same.

NCAR and GFDL are using relatively fine-mesh ocean models (mesh size 1°–1.125° in zonal direction), but the grid distortion in the northern North Atlantic apparent in Figs. 11 and 12 is not conducive to resolving spatial details in the downwelling pattern there.

As in Fig. 10, we see in Figs. 11 and 12 a somewhat patchy structure of diapycnal motion in the downwelling region of the Atlantic MOC. Overall, the geographic distribution of the up and downwelling centers in the control run in both NCAR and GFDL is remarkably similar to that in the CO_2 doubling runs. The same can be said for the Southern Ocean.

Talley et al. (2003), in their analysis of observational data, find a North Pacific deep overturning cell which they call "perplexing" and "puzzling". Qualitatively similar cells are seen in the results from the two GISS models (Figs. 5 and 6). In GISS EH this cell is associated with water mass conversion processes near the Kamchatka peninsula (Fig. 9), presumably related to cold-air outbreaks from eastern Siberia. In GISS ER, most of

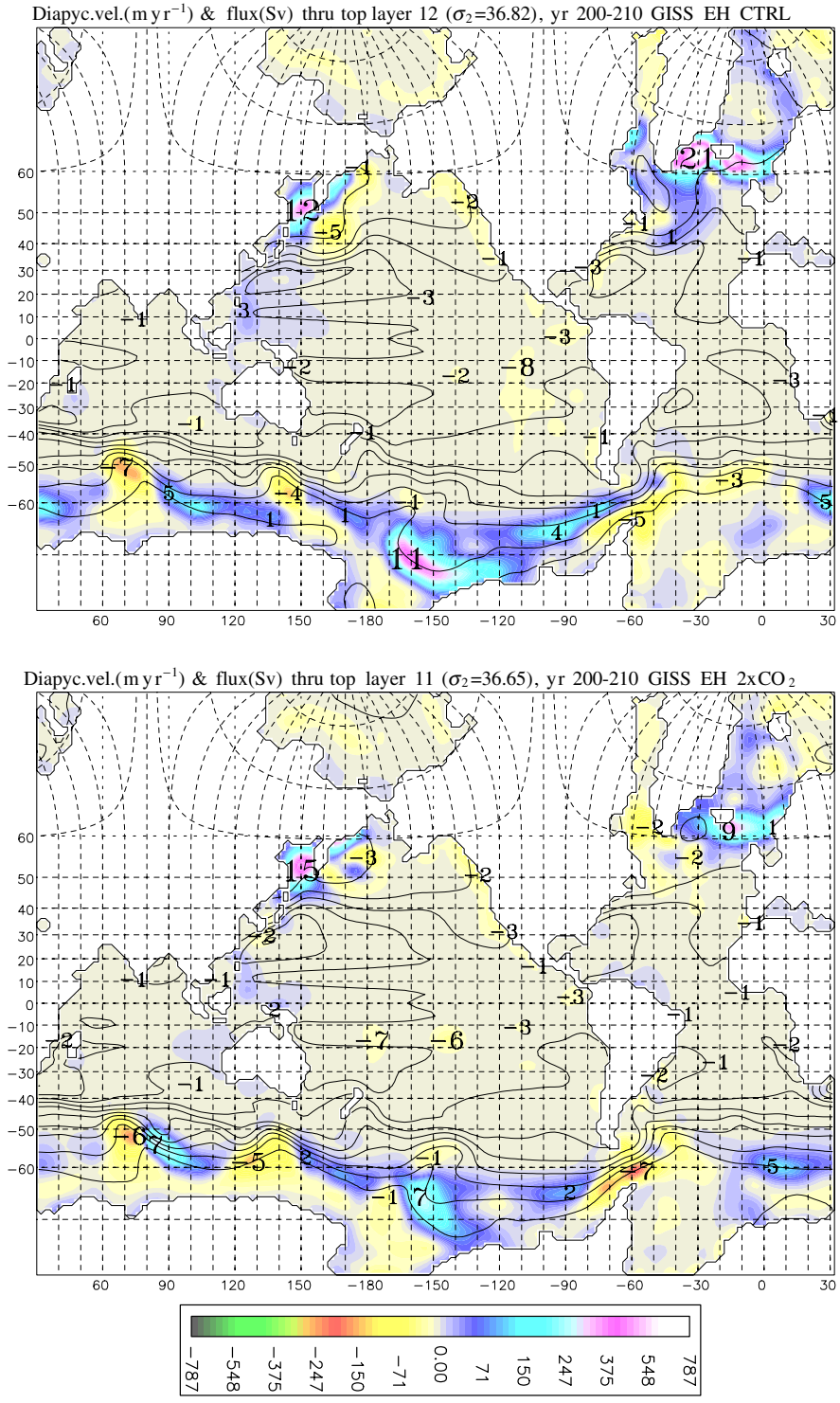

Fig. 9. Diapycnal fluxes from control run (upper) and CO_2 doubling run (lower) in GISS EH. Color contours: time-averaged diapycnal motion (m year^{-1}, positive downward) through isopycnic interface coinciding with maximum Atlantic overturning stream function value (Fig. 5). Bold numbers: Diapycnal transport (Sv), obtained by integrating over individual patches of diapycnal motion. Plain isolines: Sea surface height (contour interval 20 cm). Dashed lines: Latitude/longitude. Height/width ratio of plot matches ratio of grid points in the two directions.

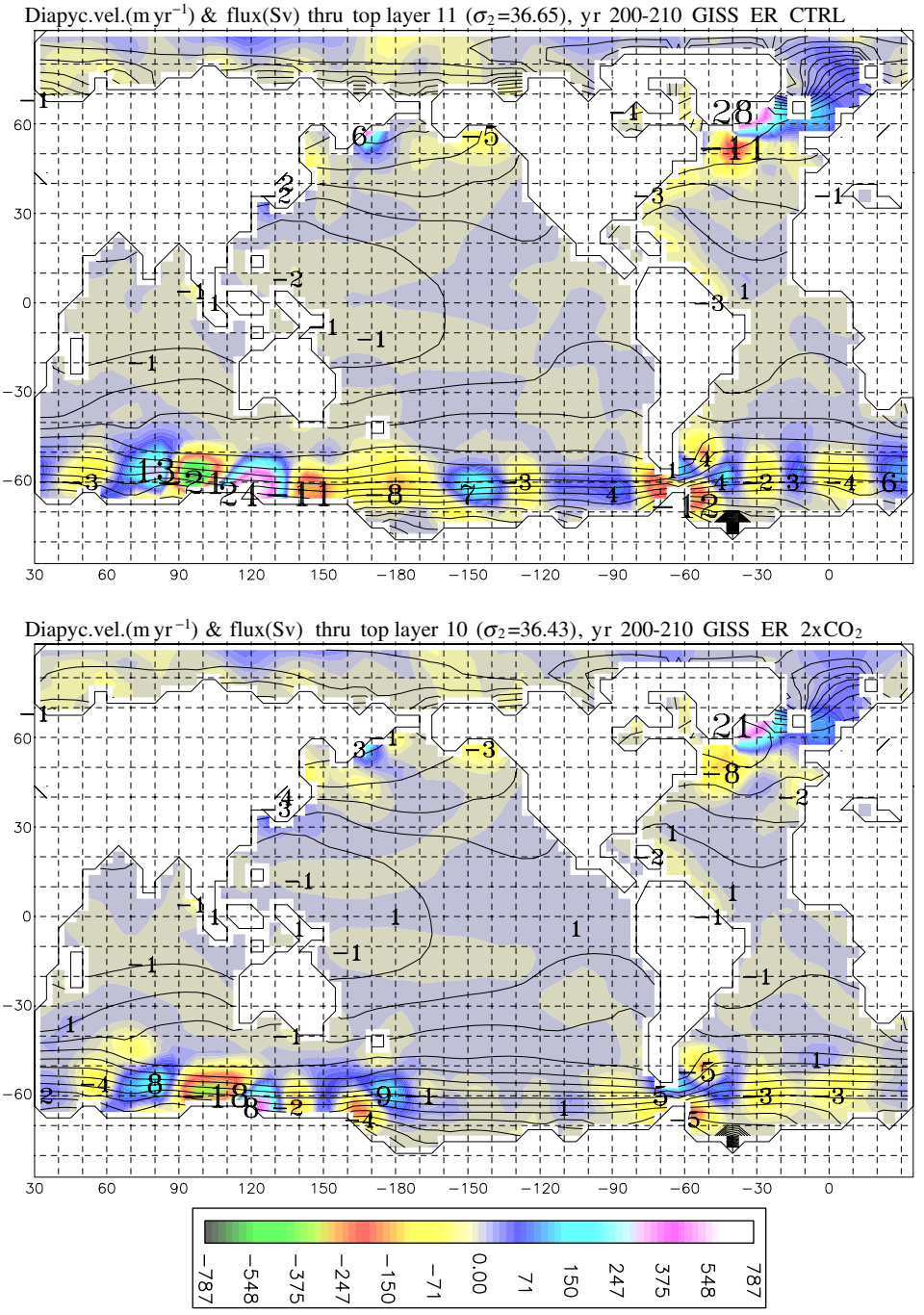

Fig. 10. As in Fig. 9, but for GISS ER model.

the downwelling takes place in the Bering Sea (results not shown). The possible connection between this cell and the one discussed by Talley et al. (2003) will be the subject of future work.

The term Veronis effect (Veronis, 1975) describes the inadvertent horizontal mixing of buoyancy across tilted baroclinic zones in z coordinate models. The resulting diapycnal upwelling/downwelling pattern on the cyclonic/anticyclonic side, respectively, of major ocean currents is quite noticeable in Fig. 11 and even

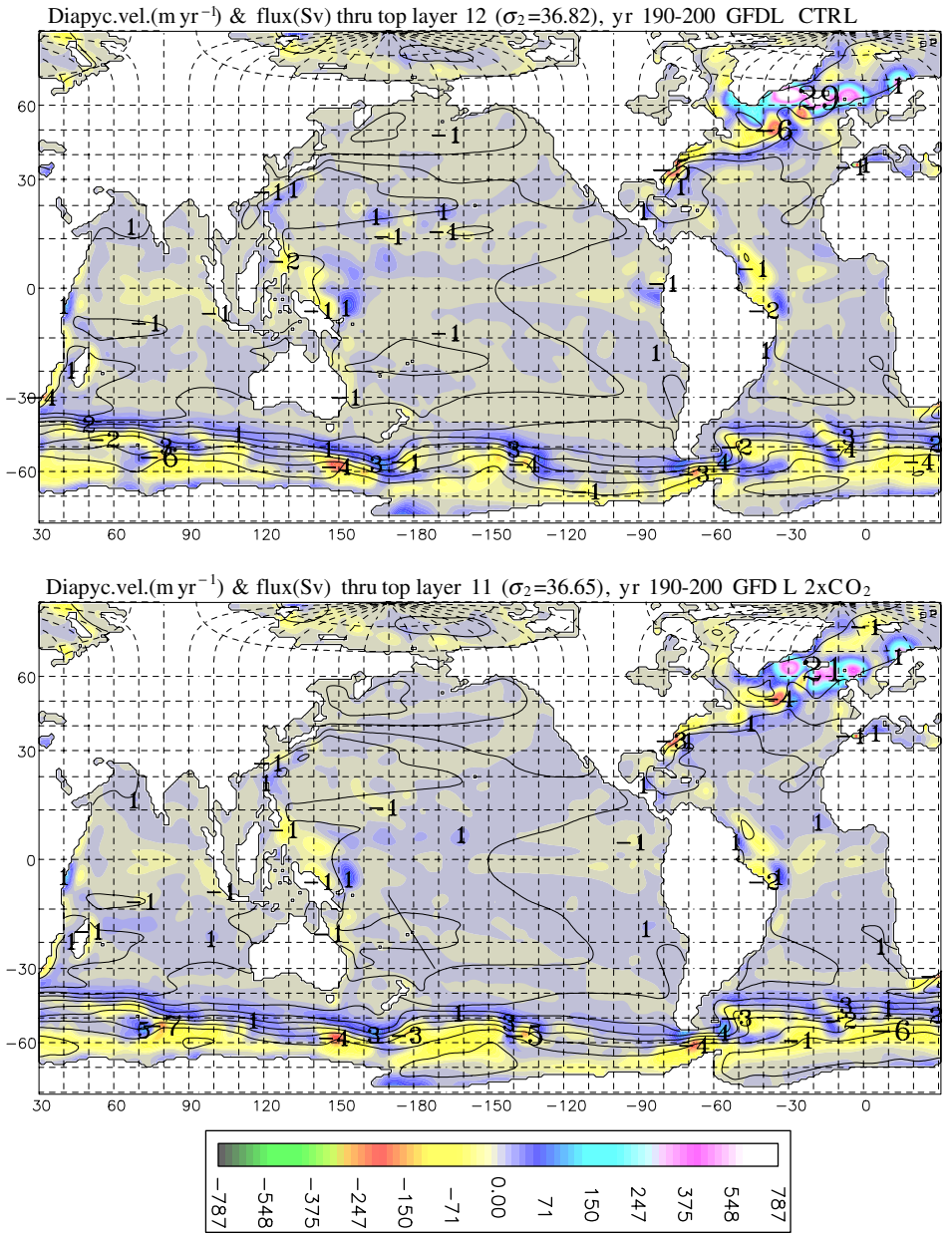

Fig. 11. As in Fig. 9, but for GFDL CM2.1 model.

more so in Fig. 12. In the Southern Ocean, the parallel bands of up and downwelling aligned with the ACC are yet another expression of the southern overturning cell seen in Figs. 7 and 8.

We surmise that the Veronis effect shows up strongly in these plots because z model velocity archives typically do not include the GM-induced bolus velocity component. This leads to a potential inconsistency in our z-to-ρ transform procedure: the layer thickness terms (Δp) in (2) are based on mass fields whose evolution is governed in part by GM-induced temperature and salt fluxes, but the velocities used in evaluating the horizontal flux terms ($\bar{\mathbf{v}}\Delta\mathbf{p}$) do not capture the GM contribution. We intend to research this issue further but find that accessing the bolus flux archives at the various institutions is not an easy matter. Furthermore, it remains to be seen whether the z models evaluate the bolus fluxes numerically in such a way that incorporating them in the horizontal flux terms will maintain the spatial coherence of the residual term ($\dot{s}\partial p/\partial s$) which we see in our present work.

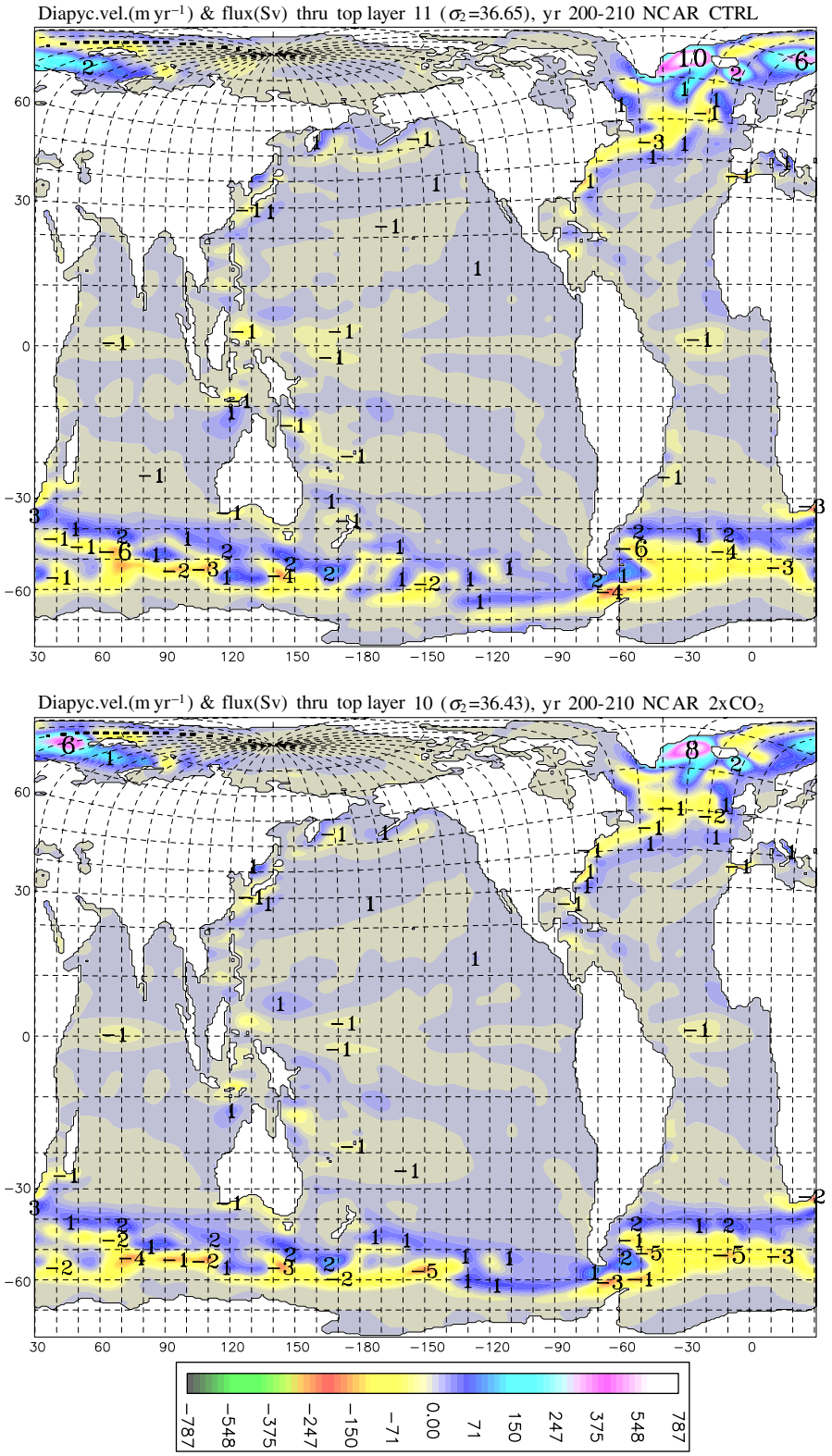

Fig. 12. As in Fig. 9, but for NCAR CCSM3 model. Height/width ratio of plot reduced by 1/3 to fit page.

One conspicuous feature in Figs. 9–12 is the concentration of diapycnal downwelling in the vicinity of the Greenland–Iceland–Scotland (GIS) ridge. Since numerically induced diapycnal mixing in dense overflows is a known problem in z coordinate models, the question arises whether the enhanced descent (in density space) in that particular region is in any way related to spurious vertical mixing rather than heat loss at the sea surface.

Resolution limitations do not allow us to settle this question on the basis of the material presented in Figs. 9–12, but some insight can be gained by supplementing the stream function plots with 3-D mass flux diagnostics. This is the topic of the following section.

4.4. Overflow across the Greenland–Iceland–Scotland ridge

The overflow from the Greenland–Iceland–Norwegian (GIN) Sea is an important part of the Atlantic MOC; it contributes about 6 Sv of the densest water to the southward return flow (Dickson and Brown, 1994; Wood et al., 1999). Turbulent mixing near the overflow sills in the Denmark Strait and the Faeroe Bank (FB) channel is a vital link in the chain of events leading to the formation of North Atlantic deep water (NADW). Hence, proper simulation of the MOC as a whole requires proper simulation of the density changes associated with overflow mixing. Note that none of the four models analyzed here has the spatial resolution that would allow it to explicitly simulate turbulent exchange processes in the descending overflow plume.

We base our discussion of the various renditions of GIN Sea overflow on regional plots of (a) the horizontal flux in the 2–5 lowest isopycnic layers that feed water across the ridge, and (b) the diapycnal flux through the interface capping those layers. The plots are shown in Fig. 13 for the control run (left 2 columns) and the $2 \times CO_2$ run (right 2 columns). The strings of arrows marking the various pathways of water in the region around Iceland are based on the Bleck and Sun (2004) streamline-bundling technique mentioned earlier. The numbers next to arrows indicate the mass flux transport in Sv. The layer combination for which isopycnic flux arrows were constructed was chosen on the basis of the interface showing the largest upward diapycnal mass flux downstream of the GIS ridge. In no case was there GIN sea outflow in layers above that particular interface.

In the control run, both ocean models coupled to the GISS atmospheric and sea ice model show downwelling in the GIN Sea into the bottom layers off Norway at the rate of 4 Sv. Roughly half of that water flows southwestward across the GIS ridge and upwells there into lighter layers. The fact that the two ocean models agree on yielding a rather weak overflow rate suggests that the root of this weakness may lie within the atmospheric and sea ice component.

In the GFDL and NCAR model, the overflow strength is 6 Sv and 5 Sv, respectively, in excellent agreement with observational estimates. The fact that outflow in the GFDL model takes place exclusively through the Denmark Strait is most likely a sill depth issue. The Denmark Strait sill is deeper in the GFDL than the NCAR model (985 versus 644 m), but GFDL's Faeroe Bank channel is much shallower (378 versus 814 m).

A prominent feature in all four models is the virtually total conversion of isopycnal into diapycnal mass fluxes downstream of the GIS sill. This conversion from "horizontal" to "vertical" in our analysis marks the dilution of overflow water by lighter ambient water in the northern Irminger Sea. The annually averaged speed at which water rises through the isopycnal interface, indicated in Fig. 13 by color contours, is seen to exceed values of 2 km/year or 0.06 mm s^{-1} in some places in the GFDL and NCAR model.

Plots of vertical displacement through isopycnic interfaces higher up in the water column (not shown here) indicate that the upward motion shown in Fig. 13 is vertically separate from the patches of downward motion seen in Figs. 9–12. The fact that the models anchor the descending branch of the Atlantic MOC in the same general area where bottom turbulence causes water masses to ascend in density space therefore seems coincidental, i.e., does not seem to imply a direct physical connection.

The strength of near-bottom overflow mixing in the two GISS models is reduced in the CO_2 doubling runs (upper right quadrant in Fig. 13). We attribute this to the shift toward lower densities in the southward-flowing branch of the Atlantic MOC, shown in the lower left panels in Figs. 5 and 6. This density shift, accompanied by a general decline in the rate at which water cycles through the GIN basin, appears to inhibit water from sinking to sufficient depths to interact with the bottom and thereby be subjected to overflow mixing.

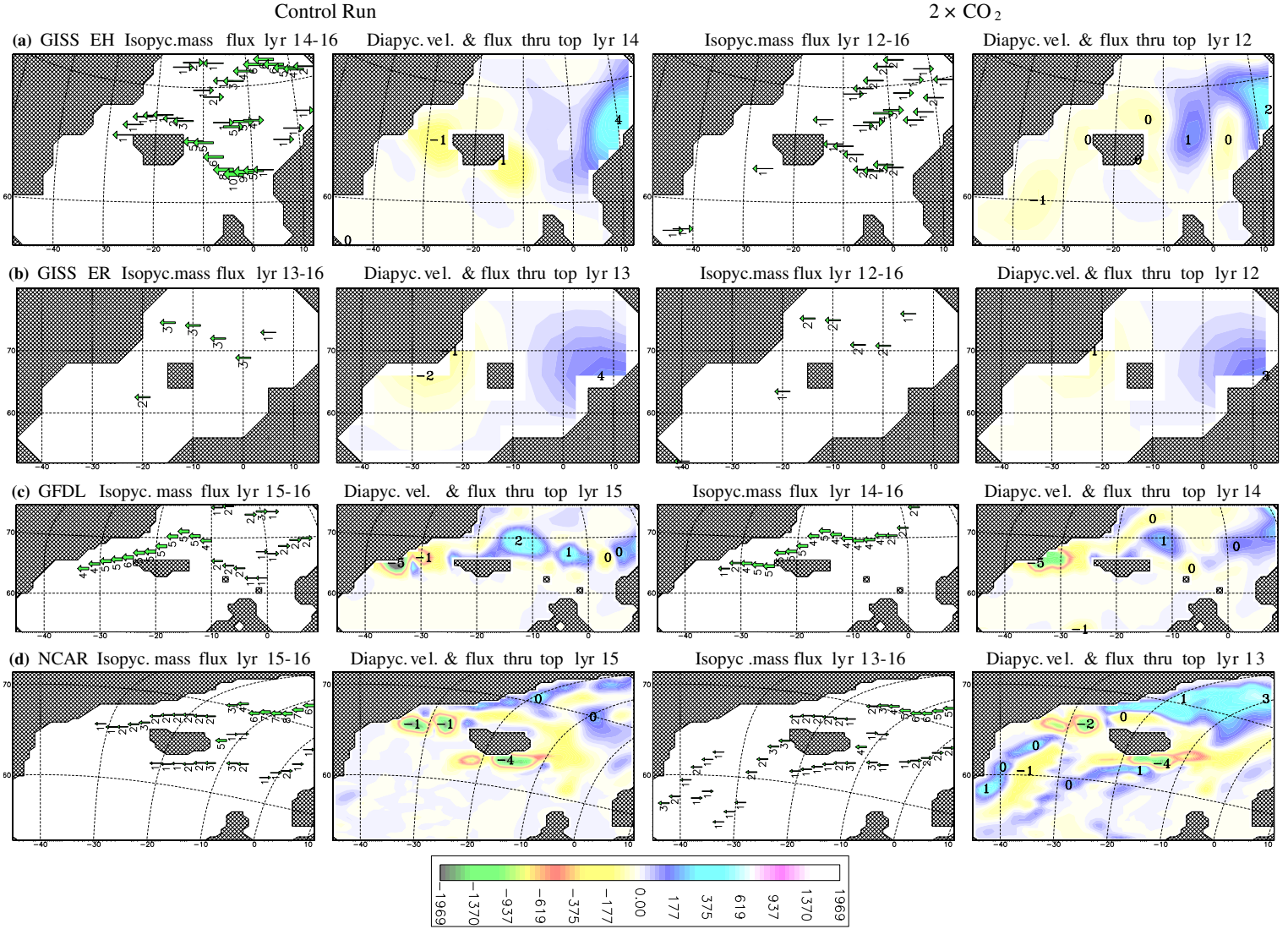

Fig. 13. Isopycnal mass flux (Sv in number next to green arrow) in the layers where the overflow across the Greenland–Scotland ridge occurred, and diapycnal velocity (m year^{-1} in color) and diapycnal flux (Sv in number) at the interface above, in all four models, GISS EH, GISS ER, GFDL and NCAR, in the control run and the 2 × CO_2 run, respectively.

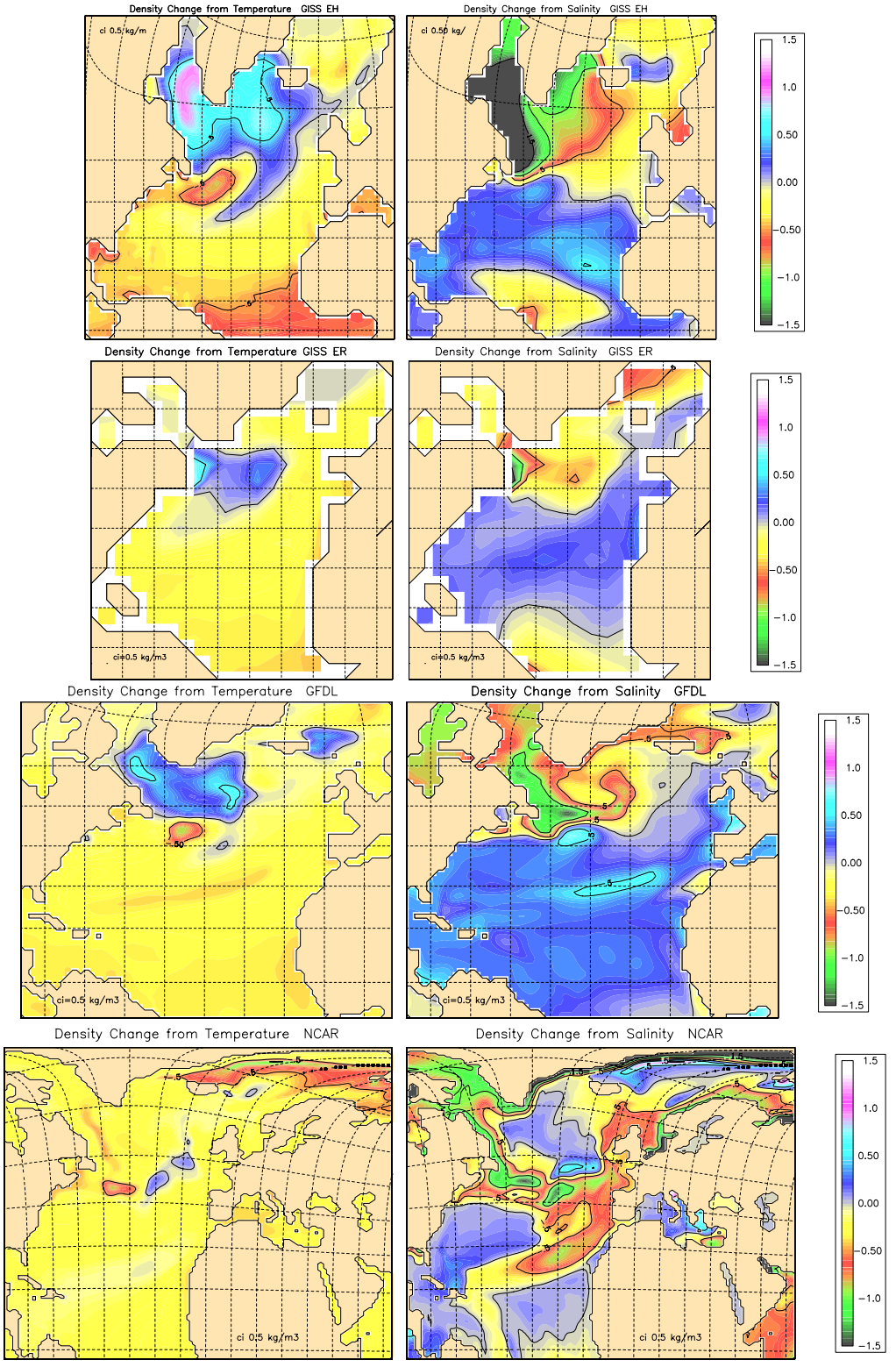

Fig. 14. Surface density change (kg m^{-3}) resulting from temperature change [$\delta\sigma_0(T)$] (left column) and salinity change [$\delta\sigma_0(S)$] (right column) in the CO_2 doubling run relative to control run in the GISS EH, GISS ER, GFDL CM2.1 and NCAR CCSM3 models (top to bottom). Dashed lines: latitude/longitude.

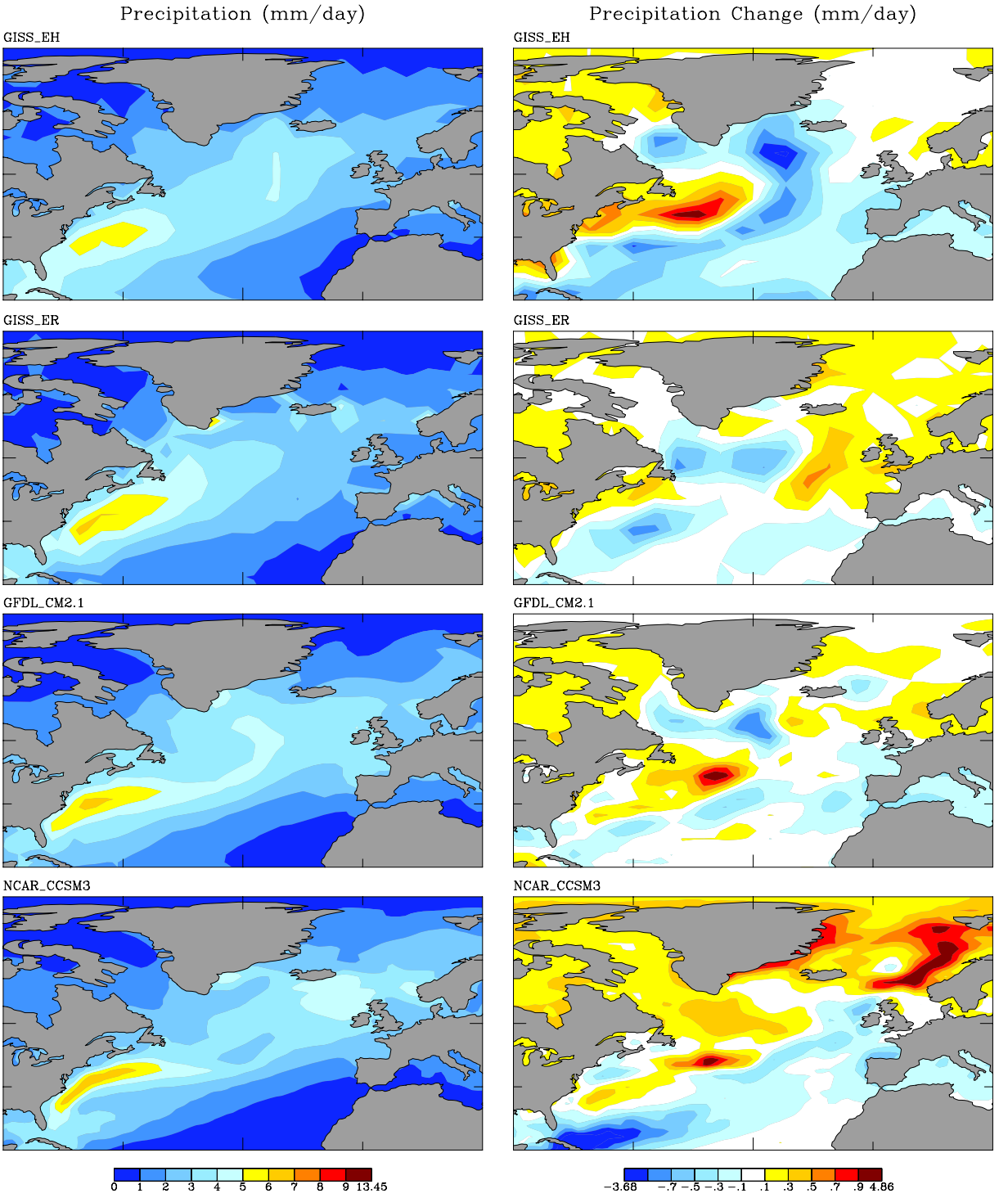

Fig. 15. Precipitation (mm day^{-1}) in the control run (left column) and its change in the CO_2 doubling run (right column) in the four models.

In contrast to the above, CO_2 doubling has no noticeable effect on the strength of overflow mixing in the GFDL and NCAR CO_2 model runs (lower right quadrant in Fig. 13). Despite the fact that the diapycnal flux

reaches its maximum at lower densities, the GIN Sea outflow in these two models still appears to occur at levels where it is spawns bottom turbulence.

4.5. Climate connections

To answer the question of whether surface freshwater or heat flux changes are responsible for slowing down the THC during global warming, some studies have tried to change one forcing at a time (e.g., Dixon et al., 1999). This is not an option here when analyzing data from different modeling groups. Instead, we decided to attribute the modeled surface density trends during global warming to contributions from temperature and salinity trends by using a linearized equation of state.

If surface density is approximated by:

$$\sigma_0 = c_1 + c_2 T + c_3 S,$$

where $c_1 = 0.166$ kg/m^3, $c_2 = -0.205$ kg/(m^3 deg), $c_3 = 0.812$ kg/(m^3 psu), while T, S and σ_0 represent temperature, salinity and potential density referenced to the surface, then the individual contributions of temperature and salinity changes to the overall density change in the CO_2 doubling case can be estimated from:

$$\delta\sigma_0(T) = c_2 \delta T,$$
$$\delta\sigma_0(S) = c_3 \delta S,$$

where δT and δS are the temperature and salinity increments in the CO_2 doubling run compared to the control run.

The density change components resulting from this decomposition are shown in Fig. 14. The total changes in surface density resulting from the T/S changes accompanying the doubling of atmospheric CO_2 content are not shown but can be inferred in the case of the northern North Atlantic from the leftmost panels in Figs. 5–8. These panels show that doubling of CO_2 in all four models causes the deep southward flow in the Atlantic to become lighter by at least one density class. The surface density field in the sinking region(s) must reflect this change. Given that cooling (warming) of surface waters is accompanied, in a broad-brush sense, by freshening (salting), the density loss in the sinking region of the North Atlantic due to CO_2 doubling can be expected to be caused by either excessive warming combined with moderate salting, or excessive freshening combined with moderate cooling.

Fig. 14 clearly shows the compensating effect of salinity and temperature trends on water density just mentioned, but in the main sinking region around Iceland, freshening appears to be the dominant process. The density loss due to freshening of the Irminger Sea is particularly strong in GISS EH, consistent with the substantial decrease in overturning strength seen in Fig. 5.

The precipitation fields displayed in Fig. 15 indicate that, with the possible exception of the NCAR model, the salinity decrease in the main sinking region is not caused by increased precipitation. Two other processes could cause the freshening, namely, reduced import of saline water into a region that on average sees more precipitation than evaporation, and a lower evaporation rate due to cooler temperatures. The negatively correlated patterns of T, S effects on density seen in Fig. 14 suggest that reduced evaporation plays the leading role. The freshening due to lower heat import from lower latitudes acts as a positive feedback on the MOC, which helps explain the sensitivity of the modeled MOC to surface boundary conditions.

In contrast to the other three models, the NCAR model predicts that CO_2 doubling will lead to rather uniform warming of the North Atlantic south of 65°N, with even stronger warming farther north (left bottom panel in Fig. 14). In both North Atlantic downwelling centers depicted in Fig. 12, one located in the Irminger Sea and one south of Spitsbergen, the density decrease appears to be due to warming (right and left bottom panels in Fig. 14).

5. Summary

A diagnostic tool originally designed to extract diapycnal mass fluxes from isopycnic-coordinate ocean model output has been used to study the geographic layout of thermohaline-forced overturning circulations

in four coupled ocean–atmosphere models participating in the current round of IPCC climate assessments. Three of those models use a fixed Cartesian grid while the fourth one uses a generalized vertical coordinate combining isopycnic coordinate representation in the ocean interior with z coordinate representation near the surface. The algorithm proves capable of yielding robust, meaningful results even when applied to z model output.

We find that in three of the four models the downwelling in the Atlantic meridional overturning circulation takes place on either side of the Greenland–Iceland–Scotland ridge, i.e., in the Irminger Sea and the southern GIN (Greenland–Iceland–Norwegian) Sea. The single exception is the NCAR model where the GIN Sea downwelling center is shifted northward toward Spitsbergen. While increasing CO_2 concentration in the atmosphere to twice the initial value at the rate of 1% per year weakens the Atlantic MOC in all models, the downwelling takes place in roughly the same location(s) as in the control runs.

The GISS EH model, which uses the hybrid coordinate ocean model HYCOM for its ocean component, shows a much more dramatic slowdown of the Atlantic MOC at year 200 than the three z coordinate models. The phenomena accompanying this slowdown, such as major freshening of the high-latitude North Atlantic, are therefore more visible in GISS EH than in the other models. The behavior of GISS EH in this regard is actually somewhat atypical. Earlier simulations of HYCOM coupled to the GISS AGCM, as well as a host of ocean-only experiments conducted over the past decade, have created the (perhaps false) impression that MOCs are more robust in isopycnic than in z coordinate models. Given the vast scale range over which physical processes cannot be resolved explicitly in today's ocean models, we have learned since then that model results are sensitive not only to the vertical grid structure (isopycnic versus z) but to a host of physical closure assumptions. In light of our latest result, it is fair to say that, at least from the HYCOM perspective, the stability of the Atlantic MOC remains a "loose cannon" in century-scale climate prediction.

Detailed analysis of the isopycnal and the diapycnal mass fluxes in the overflow from the GIN Sea reveals a virtually total conversion of the isopycnal into diapycnal mass flux downstream of the GIS sill in all models. This conversion reflects the extensively studied entrainment of lighter water into the dense overflow plume (e.g., Dickson and Brown, 1994). According to Swift (1984), the (potential) density loss of the GIN Sea overflow due to diapycnal mixing is about 0.2–0.3 kg m^{-3}, and this overflow contributes water in the range $36.98 \leqslant \sigma_2 \leqslant 37.104$ to NADW off the continental margin of North America. It is informative to compare this with the final density of the GIN Sea overflow in the control run in the four models. The overflow in the two GISS models, although at 2–3 Sv weak to begin with, ascends into layer 13 ($\sigma_2 = 36.95$) in GISS EH, and into layer 11 ($\sigma_2 = 36.65$) in GISS ER. The latter density is outside the NADW range quoted by Swift (1984). In both the GFDL and the NCAR model, the overflow ends up with 1 Sv in layer 14 ($\sigma_2 = 37.05$) and 2–3 Sv each in layers 12 and 13 ($\sigma_2 = 36.82$ and 36.95, respectively). As in the case of GISS ER, this suggests excessive diapycnal mixing of the overflow plume by the GFDL and NCAR ocean models.

Armed with the knowledge of where in the North Atlantic the MOC waters sink in the various models, we have tried to shed light on the question of whether freshening or warming of the surface waters is responsible for the predicted MOC slowdown during CO_2-induced global warming. Our analysis shows that in three of the four models the surface density loss in the sinking region (or regions) is predominantly due to freshening. Only in the NCAR model are the downwelling regions affected mainly by warming. This is consistent with findings of Stouffer et al. (2006) and Bryan et al. (2006).

It is worth noting that our simple analysis does not answer the question of whether freshening or warming is the cause of the MOC slowdown. Once the slowdown process is underway, the positive feedback loop "MOC slowdown $\Rightarrow$ reduced poleward salt/heat transport $\Rightarrow$ freshening due to rain and reduced evaporation $\Rightarrow$ further MOC reduction" quickly obliterates the signal initiating the process.

Acknowledgements

We thank L. Nazarenko and K. Lo at GISS as well as the modeling groups at GFDL and NCAR for providing data on each model's native grid. G. Schmidt made mass fluxes available from GISS ER. F. Bryan provided NCAR data in Fig. 2d. Primary support for this project is provided by the US Climate Variability and Predictability Program (CLIVAR) (http://www.usclivar.org/index.html). RB's work was supported by the Climate Change Prediction Program administered by the Office of Science in the US Department of Energy.

References

Bleck, R., 2002. An oceanic general circulation model framed in hybrid isopycnic-Cartesian coordinates. Ocean Modelling 4, 55–88.

Bleck, R., 2006. On the use of hybrid vertical coordinates in ocean circulation modeling. In: Chassignet, E., Verron, J. (Eds.), An integrated view of oceanography: Ocean weather forecasting in the 21st century. Kluwer Academic Publishers, Dordrecht, pp. 109–126.

Bleck, R., Sun, S., 2004. Diagnostics of the oceanic thermohaline circulation in a coupled climate model. Global and Planetary Change 40, 233–248.

Broecker, W.S., 1991. The great ocean conveyor. Oceanography 4, 79–89.

Bryan, F. et al., 2006. Response of the North Atlantic thermohaline circulation and ventilation to increasing carbon dioxide in CCSM3. Journal of Climate 19, 2382–2397.

Collins, W. et al., 2006. The community climate system model: CCSM3. Journal of Climate 19, 2122–2143.

Cunningham, S.A., Alderson, S.A., King, B.A., Brandon, M.A., 2003. Transport and variability of the Antarctic circumpolar current in drake passage. Journal of Geophysical Research 108 (C5), 8084. doi:10.1029/2001JC00114.

Danabasoglu, G., Large, W.G., Tribbia, J.J., Gent, P.R., 2006. Diurnal coupling in the tropical oceans in CCSM3. Journal of Climate 19, 2347–2365.

Delworth, T.L. et al., 2006. GFDL's CM2 global coupled climate models – Part 1: Formulation and simulation characteristics. Journal of Climate 19, 643–674.

Dickson, R.R., Brown, J., 1994. The production of North Atlantic deep water: Sources, rates and pathways. Journal of Geophysical Research 99, 12319–12341.

Dixon, K.W., Lanzante, J.R., 1999. Global mean surface air temperature and North Atlantic overturning in a suite of coupled GCM climate change experiments. Geophysics Research Letters 26, 1885–1888.

Dixon, K.W., Delworth, T.L., Spelman, M.J., Stouffer, R.J., 1999. The influence of transient surface fluxes on North Atlantic overturning in a coupled GCM climate change experiment. Geophysics Research Letters 26, 2749–2752.

Fyfe, J., Saenko, O., 2005. Human-induced change in the Antarctic circumpolar current. Journal of Climate 18, 3068–3073.

Ganachaud, A., Wunsch, C., 2000. Improved estimates of global ocean circulation, heat transport and mixing from hydrographic data. Nature 408, 453–457.

Gent, P., 2001. Will the North Atlantic Ocean thermohaline circulation weaken during the 21st century? Geophysics Research Letters 28, 1023–1026.

Gent, P., McWilliams, J.C., 1990. Isopycnal mixing in ocean circulation models. Journal of Physical Oceanography 20, 150–155.

Gnanadesikan, A. et al., 2006. GFDL's CM2 global coupled climate models – Part 2: The baseline ocean simulation. Journal of Climate 19, 675–697.

Houghton, J.T., Ding, Y., Griggs, D.J., Noguer, M., van der Linden, P.J., Dai, X., Maskell, K., Johnson, C.A. (Eds.), 2001. Climate Change. The scientific basic. Contribution of working group I to the third assessment report of the intergovernmental panel on climate change (IPCC). Cambridge University Press, Cambridge, p. 881.

Hu, A., Meehl, G.A., Washington, W.M., Dai, A., 2004. Response of the Atlantic thermohaline circulation to increased atmospheric CO_2 in a coupled model. Journal of Climate 17, 4267–4279.

Kraus, E.B., Turner, J.S., 1967. A one-dimensional model of the seasonal thermocline, II. The general theory and its consequences. Tellus 19, 98–105.

Large, W., McWilliams, J., Doney, S., 1994. Oceanic vertical mixing: A review and a model with a nonlocal boundary layer parameterization. Review of Geophysics 32, 336–403.

Latif, M., Roeckner, E., Mikolajewicz, U., Voss, R., 2000. Tropical stabilization of the thermohaline circulation in a greenhouse warming simulation. Journal of Climate 13, 1809–1813.

Macdonald, A.M., Wunsch, C., 1996. An estimate of global ocean circulation and heat fluxes. Nature 382, 436–439.

Mikolajewicz, U., Voss, R., 2000. The role of the individual air–sea flux components in CO_2-induced changes of the ocean's circulation and climate. Climate Dynamics 16, 627–642.

Olbers, D., Borowski, D., Völker, C., Wolff, J.-O., 2004. The dynamical balance, transport and circulation of the Antarctic Circumpolar Current. Antarctic Science 16 (4), 439–470.

Russell, G.L., Miller, J.R., Rind, D., Ruedy, R., Schmidt, G., Sheth, S., 2000. Comparison of model and observed regional temperature changes during the past 40 years. Journal of Geophysical Research 105, 14891–14898.

Schmidt, G. et al., 2006. Present day atmospheric simulations using GISS ModelE: Comparison to in-situ, satellite and reanalysis data. Journal of Climate 19, 153–192.

Schmitz Jr., W.J., 1995. On the interbasin-scale thermohaline circulation. Review of Geophysics 33, 151–173.

Steele, M., Morley, R., Ermold, R., 2001. PHC: A global ocean hydrography with a high-quality Arctic Ocean. Journal of Climate 14, 2079–2087.

Stouffer, R. et al., 2006. GFDL's CM2 global coupled climate models – Part 4: Idealized climate response. Journal of Climate 19, 723–740.

Sun, S., Bleck, R., 2001a. Atlantic thermohaline circulation and its response to increasing CO_2 in a coupled atmosphere–ocean model. Geophysics Research Letters 28, 4223–4226.

Sun, S., Bleck, R., 2001b. Thermohaline circulation studies with an isopycnic coordinate ocean model. Journal of Physical Oceanography 31, 2761–2782.

Sun, S., Bleck, R., 2006. Multi-Century simulations with the coupled GISS-HYCOM climate model: Control experiments. Climate Dynamics 26, 407–428.

Swift, J.H., 1984. The circulation of the Denmark Strait and Iceland–Scotland overflow waters in the North Atlantic. Deep Sea Research 31, 1339–1355.

Talley, L., Reid, J.L., Robbins, P.E., 2003. Data-based meridional overturning streamfunctions for the global ocean. Journal of Climate 16, 3213–3226.

Thorpe, R.B., Gregory, J.M., Johns, T.C., Wood, R.A., Mitchell, J.F.B., 2001. Mechanisms determining the Atlantic thermohaline circulation response to greenhouse gas forcing in a non-flux-adjusted coupled climate model. Journal of Climate 14, 3102–3116.

Veronis, G., 1975. The role of models in tracer studies. Numerical Models of the Ocean Circuits, National Academy of Sciences, 133–146.

Whitworth, T., Peterson, R.G., 1985. Volume transport of the Antarctic Circumpolar Current from bottom pressure measurement. Journal of Physical Oceanography 15, 810–816.

Wiebe, E.C., Weaver, A.J., 1999. On the sensitivity of global warming experiments to the parameterisation of sub-grid scale ocean mixing. Climate Dynamics 15, 875–893.

Wood, R.A., Keen, A.B., Mitchell, J.F.B., Gregory, J.M., 1999. Changing spatial structure of the thermohaline circulation in response to atmospheric CO_2 forcing in a climate model. Nature 399, 572–575.